92-G Check for updates

Copyright © 1992 by ASME

A Comparison of the Measured and Predicted Flowfield in a Modern Fan-Bypass Configuration

R. K. GOYAL
Allison Gas Turbine Division, General Motors Corporation
Indianapolis, IN 46206-0420

W. N. DAWES
Whittle Laboratory University Engineering Department
Cambridge, UK

ABSTRACT

A 3-D viscous Navier-Stokes flow solver was used to predict core and bypass rotor performance and radial flow characteristics of a 4.6:1 bypass ratio, single stage fan. The 3-D flow solver can handle several blade rows simultaneously and has the capability to include a downstream splitter. Results of the analysis are compared with experimental data obtained during rig testing of a modern high bypass single stage turbofan in which rotor performance for both bypass and core streams was measured.

INTRODUCTION

The design of the transonic fan in a modern bypass engine is of considerable interest. Any improvement in its efficiency has a strong influence on engine thermal efficiency, while any shortfall in capacity is detrimental to the overall propulsion system efficiency. The design and analysis of the fan blade in this environment must include consideration of its interaction with the downstream flow splitter. Moreover, core stream performance and bypass duct losses are strongly impacted by fan/splitter flow interactions. It is extremely important to account for these effects in an analytical simulation of the fan system.

The simulation of the flow in multistage turbomachinery has become a topic of intense research activity in recent years. Truly unsteady simulations, while feasible technically, are far too expensive to consider for design use. Attention is therefore being given to simplified approaches, and the efforts of Dawes (1991), Adamczyk et al (1989), Cedar et al (1989) are representative of this trend. Reported herein is a comparison of experimental test data for a single stage transonic rotor with predictions using the 3-D viscous code of Dawes (1988, 1991). Calculations were made with and without the presence of a downstream flow splitter and core vane typical of a modern turbofan compression system. The experimental program was designed to provide detailed aerodynamic measurements needed for comparison with the analytical effort.

EQUATIONS OF MOTION AND SOLUTION ALGORITHM

The basic equations of motion are the fully 3-D Reynolds averaged Navier-Stokes equations expressed in cylindrical coordinates in integral conservation form:

$$\frac{\partial}{\partial t} \oint_{VOL} \overline{U} \, dVOL = \oint \overline{H} \cdot \overline{dAREA} + \oint \rho \overline{S} d VOL$$

(1)

where

$$
\overline{U} = \begin{bmatrix} \rho \\ \rho V_x \\ r\rho V_\theta \\ \rho V_r \\ \rho E \end{bmatrix}
\quad
\overline{H} = \begin{bmatrix} \rho \overline{q} \\ \rho V_x \overline{q} + \overline{\overline{\tau}} \, \hat{i}_x \\ r\rho V_\theta \overline{q} + \overline{\overline{\tau}} \, \hat{i}_\theta \\ \rho V_r \overline{q} + \overline{\overline{\tau}} \, \hat{i}_r \\ \rho I \, \overline{q} \end{bmatrix}
\quad
\overline{S} = \begin{bmatrix} 0 \\ 0 \\ -2\Omega r V_r \\ \dfrac{V_\theta^2}{r} + r\Omega^2 - 2\Omega V_\theta \\ 0 \end{bmatrix}
$$

with

$\overline{q} = V_x \hat{i}_x + V_r \hat{i}_r + V_\theta \hat{i}_\theta$, the relative velocity, and V_x, V_r, V_θ are the axial, radial and tangential relative velocities

Ω = rotational speed of rotor

$\overline{\overline{\tau}}$ = the stress tensor containing both the static pressure and the viscous stresses

and $I = c_p T_{O_{rel}} - 0.5 \, (\Omega r)^2$, the rothalpy. The system is closed by an equation of state $\rho = \rho(\gamma - 1)(E - 0.5 * (\overline{q} \cdot \overline{q} - (\Omega r)^2))$.

The turbulent viscous stresses are computed from the Baldwin-Lomax (1978) mixing length model. The implementations of the Baldwin-Lomax (BL) model in a 3-D code is described in Dawes (1987). The main point algorithmically is how to determine the velocity and length scales in the blade endwall corners. (We cannot quantify the likely errors associated with a strongly 3-D boundary layer on the fan blade with perhaps strong radial outwards migration of boundary layer fluid downstream of the shock suction surface interaction). Rather than use weighted averaging of the scales in the corners as recommended by some authors (e.g. $\ell = N(1/\ell_{suction\ side}^2 + 1/\ell_{hub}^2)$ which gives rise to too much diffusion, the cross-flow plane is divided into such zones simply on the basis of the closest wetted surface. Within each of these "triangular" zones, BL is applied along the cross-flow plane. This approach was subsequently adopted and recommended by Adamczyk, et. al. (1991). Transition, remains a substantial uncertainty and for the present work transition was fixed at the blade leading edges.

The equations are discretized on a set of six-faced control val-

ues, formed by a simple, structured H-mesh construction. Flow variables are stored at cell centers and values on cell face for flux evaluation are found by simple linear interpolation conferring second-order accuracy on smoothly varying meshes. The code solves the equations of motion using a simple and robust time-marching algorithm. The basic solution algorithm has been described in detail elsewhere (for example Dawes (1988)), and consists of a two-step explicit, one-step implicit scheme similar in implementation to a two-step Runge-Kutta method plus residual smoothing.

The Dawes code uses the "industry standard" artificial smoothing model, first introduced by Jameson, consisting of a solution-adaptive combination of second and fourth derivatives. The fourth derivative term provides background smoothing and has the form

$\varepsilon^4 |\lambda| \Delta x^3 \nabla^4 u$ and so does not distrupt the formal second order accuracy of the algorithm ($|\lambda|$) is related to the spectral radius of the equation of motion). For the current application ε^4 was set to 0.01. Near shocks, a pressure gradient switch (based on the undivided Laplacian of static pressure), turns off the fourth derivative smoothing and turns on second derivative smoothing to obtain crisp shock capture over 3-4 cells. In tests (Dawes, 1987), the overall impact of smoothing and truncation error on predicted loss coefficient was estimated to be such that 10-20% of the loss level is spurious (i.e. a predicted loss coefficient of 5% is $5 \pm 1\%$).

The basic single row analysis has recently been extended to allow simultaneous solution of several blade rows (Dawes (1991). To permit multi-row analysis in reasonable computer times, the assumption is made that the flow is steady relative to each individual blade row. Clearly, some sort of circumferential averaging must then be employed to model the relative motion of the blade rows and this averaging is implemented via inter-row "mixing planes." Any model adopted for the mixing planes represents an approximation; neverthless, it is important to note that although the circumferential information is smeared, the radial variation is not.

In the present version of the multiblade code, the mixing plane model is based on performing a classical mixing analysis at each spanwise station on either side of the mixing plane. Dring (1990) has shown in the context of throughflow analysis, that such mixing analyses are much better able to produce an "equivalent steady inlet condition" to subsequent blade rows than other forms of averaging. For compressible flow this mixing is expressed as shown below (expressed for simplicity in a mixing plane normal to the axial direction):

$$\sum \rho v_x \Delta A = \dot{m} = \widetilde{\rho} \widetilde{v_x} \overline{A}$$

$$\sum (p + \rho v_x^2) \Delta A = (\widetilde{p} + \widetilde{\rho} \widetilde{v_x^2}) \overline{A}$$

$$\sum (\rho V_x v_t) \Delta A = \widetilde{\rho} \widetilde{v_x} \widetilde{v_t} \overline{A}$$

$$\sum (\rho v_x v_r) \Delta A = \widetilde{\rho} \widetilde{v_x} \widetilde{v_r} \overline{A}$$

$$\sum \rho v_x T_{o_{abs}} \Delta A = \dot{m} \widetilde{T}_{o_{abs}}$$

$$\sum \Delta A = \overline{A}$$

where $\sum ... \Delta A$ represents a circumferential summation of area for each radial station and m is the mass flow. These five equations are solved for the five uniform mixed out flow variables (denoted by the superscript ~ to be imposed on either side of the mixing plane.

If the mixing is carried out in this way, then all the loss implicit in the nonuniform circumferential flow is mixed out explicitly into loss. Obviously not all of the nonuniformity may actually become a loss in practice as the following blade may interact favorably with its inflow. The point is that no spurious losses (or mass flow or total temperature) are introduced by the circumferential averaging process. In practice, this mixing plane formulation performs well even if the flow is separated and is coded in a more general manner than described above to permit the mixing plane to be inclined to the purely axial direction.

The governing equations are completed by specification of boundary conditions. At inflow, total pressure and temperature are fixed and either flow angle or absolute swirl velocity are held constant. At the outflow, the hub or tip static pressure is fixed and the radial

variation is derived from the simple radial equilibrium equation. For cells adjacent to solid boundaries, zero fluxes of mass, momentum, and energy are imposed through the cell face aligned with the solid boundary. Wall static pressure is calculated by setting the derivatives of pressure normal to the wall equal to zero. To prescribe the wall shear stress, the velocities stored at cell centers adjacent to the wall and the known zero value of velocity on the wall are used to compute the velocity gradients at the wall. These gradients, together with the wall viscosity, are used with a locally defined curvilinear coordinate system to compute the wall shear. If appropriate, the wall shear stress is computed from a universal logarithmic skin friction law; the code itself decides when.

TEST RIG AND INSTRUMENTATION

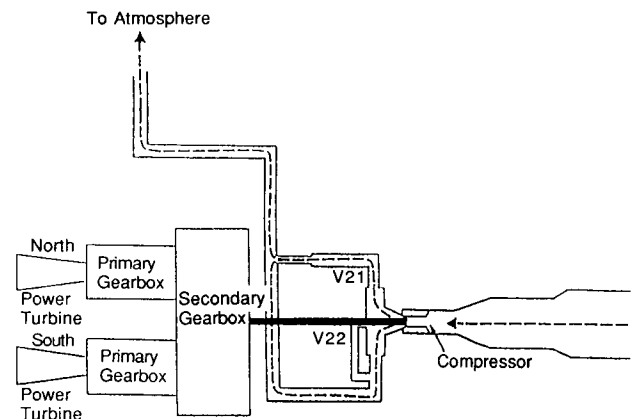A single stage fan rig arrangement (Figure 1) was used for the

Figure 1. Large compressor facility.

experimental portion of the program. Ambient air enters the inlet plenum after being metered through an adjustable orfice located in the upstream ducting. Fan drive power is provided by two J71 power turbines, which drive through two primary (and one secondary) gearboxes. From the fan discharge, the air is turned and exhausted to the atmosphere.

The fan stage is designed to produce a corrected airflow rate of the order of 300 lbs/sec. The rotor operates transonically with an inlet tip relative Mach number of 1.55. The fan rotor inlet hub/tip diameter ratio is 0.38.
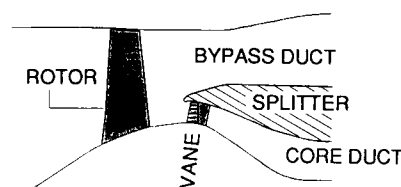
INSTRUMENTATION

Fan rotor, core and bypass vane instrumentation used during fan rig testing and the computational domain is summarized in Figure 2. The inlet plenum is instrumented with four 5-element total pressure and 4 total temperature rakes and 4 tip static pressure taps. The case instrumentation over the fan rotor has 14 in-line static pressure taps equally spaced axially: two upstream of the blade leading edge, two downstream of the blade leading edge, one each in the plane of leading and trailing edge and eight over the blade. No bleed was used on the casing of the fan rotor. The hub instrumentation at the fan rotor trailing edge consists of four static pressure taps 90 deg apart. The fan splitter nose was instrumented with two static pressure taps at each of six axial locations, each 180 deg apart pitchwise.

At plane A, the leading edge of the core vane was instrumented with total pressure probes at 5, 10, 30, 50, 70, 90, and 95 % of the vane span. (Duplicate coverage was used at each depth). Two each hub and tip wall static taps were located in the axial plane of the total instrumentation.

At the core vane mid pitch, there were two static pressure taps 180 deg apart at 50% chord, and, two static pressure taps 180 deg apart at the trailing edge of the vane. At plane B, the vane discharge was instrumented with total temperature probes at 5, 10, 30, 50, 70, 90 and 95 % of the vane span. (Duplicate coverage was used at each depth). There were two each hub and tip wall static taps. Additional instrumentation consisted of (1) hub and tip wall statics located axially

2
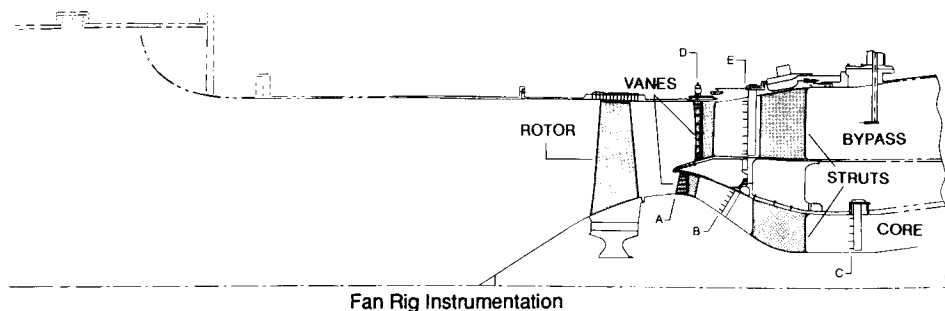
Fan Rig Instrumentation

Computational Domain

Figure 2. Fan rig instrumentation and the computational domain.

along the duct, and (2) a tip boundary layer 9-element rake located at the strut trailing edge.

The bypass vane leading edge instrumentation at plane D consisted of total pressure probes at 5, 10, 23, 36, 50, 64, 77, 90, and 95 % span (two at each depth). Two tip static pressure taps located 180 deg apart in the plane of the total pressure probes. Similarily, the bypass vane discharge instrumentation at plane E consisted of total temperature probes at 5, 10, 23, 36, 50, 64, 77, 90, and 95 % span (two at each depth). Two tip static pressure taps were positioned 180 deg apart in the plane of the total pressure probes.

Conservation of angular momentum was enforced in an axisymmetric throughflow analysis to project measured temperatures and pressures from planes A, B, D, and E to the rotor blade trailing edge. This analysis uses the method of Stratford (1978) to assess endwall boundary layers. No allowance is made for mixing of either the total temperature or pressure distribution across axisymmetric streamsurfaces.

RESULTS AND DISCUSSION

The results computed without the presence of a downstream splitter (Case A) and with splitter and core vane (Case B) as shown in Figure 3 are presented. The geometry of the fan rotor is the same for both cases. All the flow parameters are presented in normalized form. The corrected flow, total pressure ratio and efficiency are normalized with respect to overall design values of these parameters for fan rotor Type-II. A discussion in each case including fan rotor Type-II is presented in the following paragraphs.

Case A. Downstream Splitter Not Included in Computations

Two fan rotors with different blade designs were fabricated and experimentally tested. The baseline configuration, designated as Type-I utilized conventionally designed MCA (multicircular-arc) blading in the supersonic region of the blade. The second fan (Type-II) was designed incorporating precompression airfoils in the supersonic region of the blade span. Both rotors employed double circular arc blading (DCA) in the hub region.

Dawes 3-D code was used for designing both rotors. An H grid comprised of 37, 95, and 37 mesh points in the circumferential, axial, and radial directions respectively, was used for the rotor analysis. The grid sections in the mid-pitch meridional and hub and near tip blade-to-blade planes are shown in Figure 3. The mesh was clustered exponentially near the blade suction and pressure surfaces. In the radial direction, cells were concentrated near the casing and hub.

The fan rotor blade tip clearance was modelled rather approximately in the calculations. The present blade tip model used in the
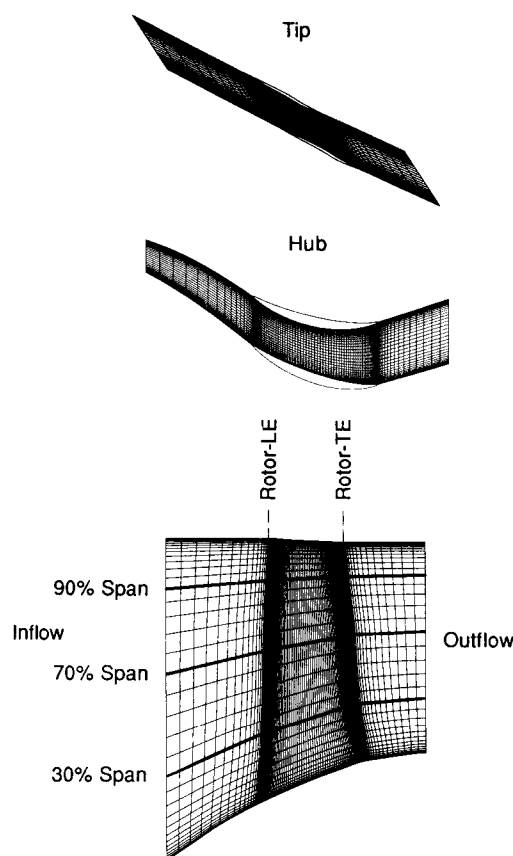

Figure 3. Meridional and blade to blade plane mesh for a fan rotor configuration (Case A, Type-II).

code (Dawes (1988)) is the so-called "pinched-tip" H-mesh model wherein the blade thickness is rapidly pinched to zero just near the tip and the casing. This is obviously a poor model for thick turbine blades but, in fact, surprisingly good for thin compressor blades. Stores and Cumptsy (1991) published a validation of the present pinched-tip model and showed good agreement with detailed experimental measurements for a compressor cascade. Basson et al (1991) published a

3

comparison of measured compressor cascade flow with predictions using a pinched-type H-mesh model and a H-mesh with an embedded mesh over the actual square blade tip. They showed little difference between the pinched-tip and embedded mesh predictions except very near the tip. In particular, global features of the clearance flow were similarly resolved by other clearance models. In terms of the number of nodes used in the clearance gap in the present study (3), Stores and Cumptsy (1991) showed, for a thin compressor blade, that even 3 nodes in the gap allowed remarkably accurate predictions of global features of the clearance flow like, for example, the axial validation of the integrated clearance leakage flow. These studies guided our engineering choice of the mesh. As stated earlier, the blade is treated in the code by simply reducing the blade thickness smoothly to zero and then applying periodic boundary conditions between the tip and the casing. A view of both fan rotors in the axial plane at 40% axial chord is shown in Figure 4. As
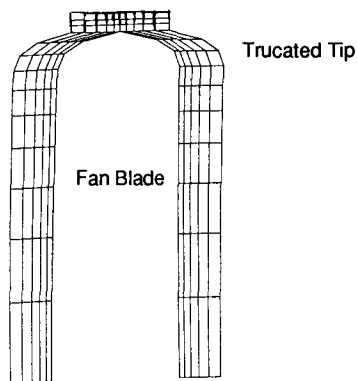

Figure 4. Near tip blade section at constant axial plane.

shown in Figure 4, the blade is truncated near the tip in three nodes. In the hot run conditions, the tip clearance was taken to be 0.04 inches which is equal to 0.37 percent of the average blade span. Only three nodes were used in the tip clearance region.

A mesh of 37 points was used in the blade-to-blade and hub-to-tip plane to simulate the boundary layers. To characterize the meshes in terms of boundary layer resolution, the mesh resolve the airfoil boundary layers down to Y+ values in the range 15-25 and the hub and casing boundary layers to 30-50. The numbers of nodes in the boundary layer region were 4 and 3 for the blade suction surface and blade pressure surface and 3 and 4 for the hub and tip endwalls respectively.

Regarding the dependency of the solution on the grid, it is difficult to establish mesh independence in 3-D flows. Ritually halving the mesh in each direction increases the CPU cost by at least a factor of 8 each time. Dawes (1988) reported a mesh refinement study for a transonic compressor cascade representative of the mid-span of a fan. Three meshes containing 17*35, 29*68 and 57*133 nodes in the blade-blade plane were used. Y+ values for the blade boundary layers were determined to be of the order of 30, 15 and 5, respectively. The predicted exit loss coefficients were shown to be essentially identical for the medium and fine meshes. This guided our current choice of meshes with 37*95 points in the blade-to-blade planes of the fan.

Design point calculations were made for both rotors. Measured values of fan inlet total pressure and total temperature were the inlet boundary conditions for the calculations. Inlet swirl was assumed to be negligible. Although the presence of an inlet tip boundary layer was detected from a boundary layer rake located 9 inches upstream of the rotor, this effect has not been included in the calculations. However, it should be noted that it is our intention to include inlet boundary layer effects into the calculations during future efforts. Cold-to-hot airfoil coordinate transformations were made using a finite element analysis as a means to account for blade untwist and shape change.

The solution was assumed to be converged when the mass flow error was within 0.4% of fan inlet flow, and the peak suction surface pressure at certain reference locations became fairly constant during the time iterations. This generally occured after 3000 iterations. To eliminate the effect of iteration count on the accuracy of the solution, the computations were continued for another 4000 iterations. (The flow, pressure ratio, and efficiency changed by -0.13%, -0.4% and -0.2% re-

spectively). From this study, it was concluded that 3000 iterations were adequate to obtain an acceptable solution. The computations were made on an IBM RS-6000 work station (Model-550) and the code processed at about 0.00022 sec/node/time step. The processing speed of a CRAY-YMP for comparison purposes is about six times faster than the Model-550.

Figures 5 and 6 show the predicted spanwise variation of pitchwise mass-averaged normalized total pressure ratio and adia-
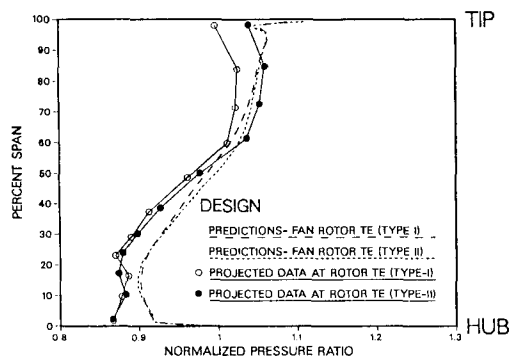

Figure 5. Predicted and measured spanwise variations of pitchwise mass-averaged total pressure ratio (fan rotor Type-I and Type-II).
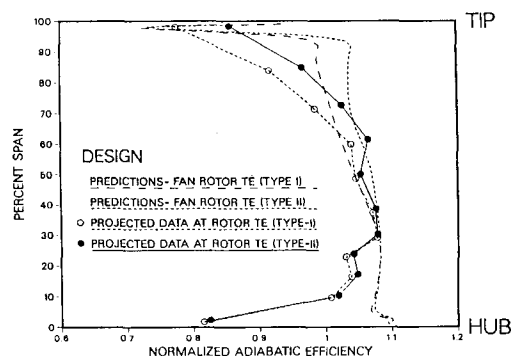

Figure 6. Predicted and measured spanwise variations of pitchwise mass-averaged adiabatic efficiency (fan rotor Type-I and Type-II).

batic efficiency at the trailing edges of Type-I and Type-II fan rotors. The predictions are compared with the data as projected to the trailing edge of the fan rotor. As previously described, the data at the rotor trailing edge was deduced from measured total pressures, temperatures at planes A, B, D, and E by enforcing conservation of angular momentum in an axisymmetric through flow analysis. No allowance is made for mixing across axisymmetric streamsurfaces. It is interesting to see in Figure 5, that the predicted radial variations in pressure ratio agree with the projected data to 75% of the span, even though the absolute levels are slightly different. Between 75 to 100% of the blade span, the computed pressure ratio for the Type-I rotor did not show any improvement over that of the Type-II rotor. The projected data showed higher pressure ratios for the Type-II blade from 75 to 98% of the span but the computations did not show such differences. The rate of change of slopes of pressure ratio near the hub and at 20% span agrees with the design intent. The overprediction of the pressure ratio in the hub region is not clearly understood at this time. This may be due to inadequacies in the turbulence model or in the numerics. Overall, the predictions and the projected data confirmed the Type-II fan design as being better than the Type-I fan design.

The spanwise variations of efficiency shown in Figure 6, indicate that the Type-II fan rotor (designed using precompression) is more efficient than the Type-I rotor. The main improvement in efficiency in the Type-II rotor design occurs outboard of 50% span when compared to the Type-I fan rotor. Such behavior is confirmed by the data. As shown in Figure 6, even though the level of spanwise variation of predicted efficiency differs from the projected data, the differences in efficiency between the Type-I and Type-II rotors are in good agreement with the

4

data. Efficiency is a very sensitive parameter to predict accurately, because a small error in temperature or pressure (either numerics or measurements) can produce a big difference in efficiency. From Figure 6, it is clear that the absolute level of predicted efficiency, if integrated radially, is higher overall than that calculated from the measurements.

Figure 7 compares the predicted spanwise variation of pitchwise mass-averaged relative flow angles and the projected data at the trailing edges of both fan rotors. The projected flow angles data showed similar behavior in both fan rotors. The computations overpredicted flow angles for both rotors compared to the projected data near 30% span. The computed flow angles were lower than the projected data near 75% span. The predicted variations of relative flow angles are consistent with the spanwise variation of total pressure ratio shown in Figure 5.

Figure 8 compares the predicted spanwise variation of pitchwise mass-averaged relative Mach numbers and the projected data at
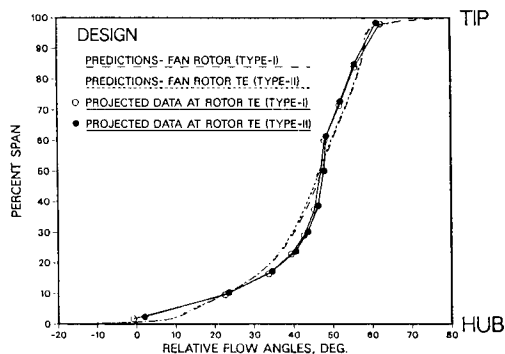

Figure 7. Predicted and measured spanwise variations of pitchwise mass-averaged relative flow angles (fan rotor Type-I and Type-II).
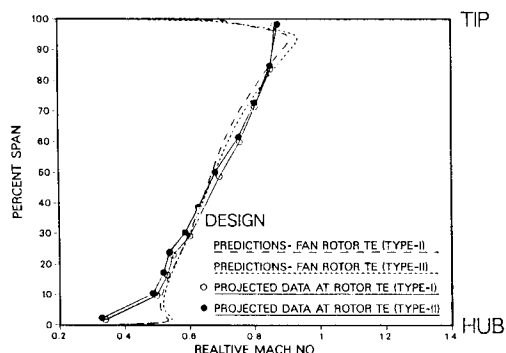

Figure 8. Predicted and measured spanwise variations of pitchwise mass-averaged relative Mach numbers (fan rotor Type-I and Type-II).

the design point. The comparison is shown at the rotor trailing edge for both fan rotors. The predicted Mach numbers compare reasonably well with the projected data except near the hub and tip. The overshoot of predicted Mach numbers near the hub and tip region is not clearly understood. The source of this descrepency is being investigated.

Figure 9 shows the predicted relative Mach number contours in the blade-to-blade plane at the design point. The contours are shown for the Type-I and Type-II fan rotors at 30%, 70%, and 90% span (approximate grid lines, see Figure 3 for clarification). In Figure 9, the sonic line is shown by the dashed lines. At 90% span, the inlet Mach numbers to the Type-I and Type-II fan rotors are 1.39 and 1.38 respectively, and exit Mach numbers are 0.89 and 0.94. It is interesting to see in Figure 9 that at 90% span, the Type-I rotor has a different shock structure than the Type-II rotor. The Type-I blade has a strong normal shock located slightly upstream of the blade trailing edge. The shock is followed by subsonic flow at the rotor exit. For the Type-II blade, a bow shock is followed by a weaker lamda shock. The shock in the Type-II blade is closer to the trailing edge than the shock in the Type-I blade. As shown in Figure 9, at 70% span from the hub, the inlet relative Mach number is 1.18 and 1.22 in the Type-I and II fan rotors, respec-
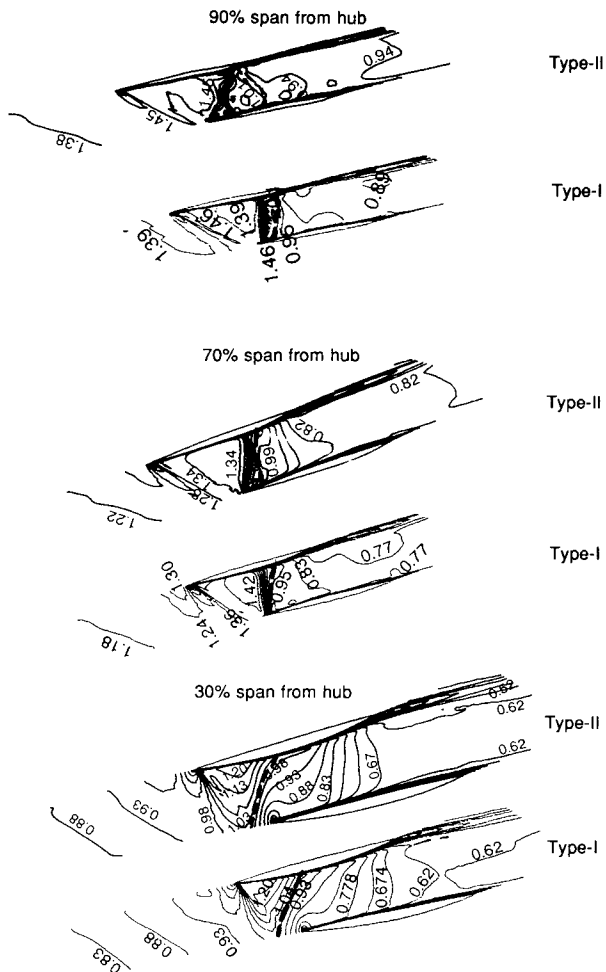

Figure 9. Comparison of predicted relative Mach number contours at 30%, 70% and 90% span for fan rotor Type-I and Type II.

tively. At 70% span, the Type-I rotor has a stronger normal shock than the Type-II rotor. The exit Mach numbers for Type-I and Type-II rotors are 0.77 and 0.82 respectively. At 30% span, the inlet Mach number is subsonic for both the rotors. A local supersonic bubble occurs on the suction surface downstream of the leading edge and this flow decelerates to a subsonic conditions after a weak shock. As antipicated (blades were redesigned in the supersonic region only), both the fan rotors did not show significant Mach number differences at 30% span.

A view of the predicted velocity vectors in the tip clearance region of the fan rotor is shown in Figure 10 for the Type-II rotor. The migration of fluid from one surface to the other is seen in the tip region.
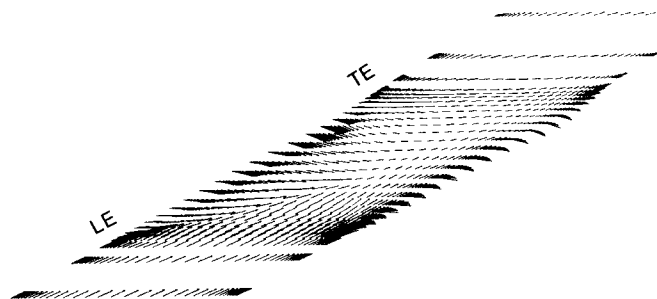

Figure 10. Predicted velocity vectors in the tip clearence region of the fan rotor Type-II.

5

Table-I shows predicted results and the deduced data for both rotors. It is significant to note that about two and one-half percentage points improvement in fan efficiency were achieved using the unconventional blade design method. Both fan rotor designs were guided by the results of the 3-D viscous analysis. The predictions and the deduced data indicated that fan rotor Type-II performed better than the Type-I fan rotor in terms of pressure ratio, efficiency, and flow.

Table-I.
Comparison of predicted and test performance- conventional MCA blading versus pre-compression blading (Type-I and Type-II).

% change (Type-II- Type-I)/Type-I*100.

	Test Data	Predictions
Rotor Pressure Ratio	1.285	0.470
Rotor Efficiency	2.5	2.800
Corrected Fan Flow	1.20	1.60

Comparisons between predicted and measured data given in the remaining text refers to the Type-II fan design configuration (with and without the presence of the downstream splitter).

Case B. Inclusion of Downstream Splitter/ Core Vane

For this case, a downstream flow splitter was modelled in the computation. The splitter divides the fan flow into the bypass and core streams as is typical for bypass engines. (Also modelled in the calculation were the stator vanes in the core stream).

The grid for the fan blade and downstream components (i.e., ducting, splitter, and core vane) was generated by combining grid systems for individual components. This was accomplished by appropriately shifting individual elements axially and tangentially to form the composite grid. The geometry of the fan rotors were identical to those of case A (Type-II) as described previously. For both cases, the fans operating tip clearance was assumed to be 0.04 inches (0.37% of the total span), which is the average value as measured during rig testing.

A structured H-mesh was constructed for the rotor as well as for the core vane and bypass duct. This was done by interpolating the input blade sections onto the desired radial set of blade-to-blade surfaces. The mesh used in the analysis was composed of 31*143*37 points. Figure 11 shows the grid in the meridional and blade-to-blade planes at hub
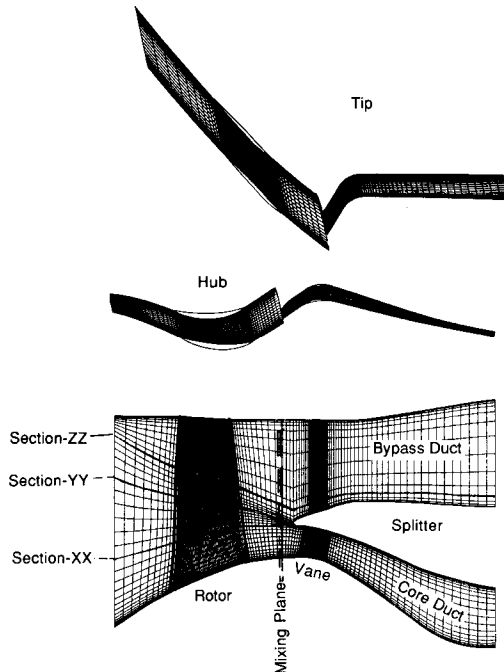
and near tip sections. The discontinuity between the fan grid and the grid for the downstream system components serve as a "dummy" boundary across which flow properties were pitchwise averaged. This was accomplished by letting the last plane of cells for the upstream domain and the first plane of cells for the downstream grid system serve as dummy storage locations for inter-row mixing calculations. The tip portion of the core vane flowpath was made to coincide with the lower boundary of the splitter, while the bypass duct was free of blading. The zero flux condition was applied on the upper and lower surfaces of the splitter and the splitter leading edge.

The 3-D computations were made for the fan bypass configuration at 100% speed from the fan operating point to near stall. For Case A, the computations were also made at the choke point. The exit static pressures at the tip of the core and bypass ducts were adjusted to define the fan speed characteristics. Because of the complex nature of this flow, the convergence for the fan bypass configuration was slower than for an isolated fan rotor. The maximum mass flow error for Case B did not go below 1.4% of the inlet mass flow as compared to 0.4% for the isolated rotor. The flow properties across the mixing plane was approximately satisfied. For case B, the numerical calculations diverged if the initial guess of the pressure was not reasonable. To avoid numerical divergence, it was very important to specify a reasonably accurate guess of pressures at the fan rotor leading and trailing edges, the inlet to core and bypass vanes, and the exit of the fan bypass ducts. In the present calculations, the initial estimates for static pressures were obtained from the axisymetric design code. The inlet flow conditions, including those for the blade tip treatment were the same as described in the earlier section.

Figures 12 and 13 show normalized total pressure ratio/airflow and efficiency/airflow characteristics as computed for Cases A and B. Also shown are data from the experimental rig test. As shown in Figures 12 and 13, the predicted fan characteristics agree well with

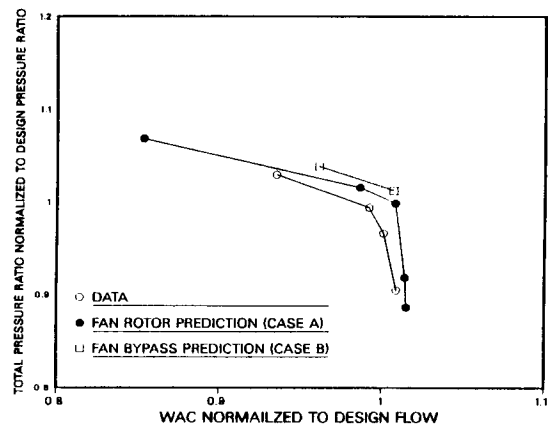Figure 11. Meridional and blade to blade plane mesh for a fan bypass configuration (Case B).

Figure 12. Comparison of measured and predicted mass-averaged total pressure ratio vs. flow (Case A & B).
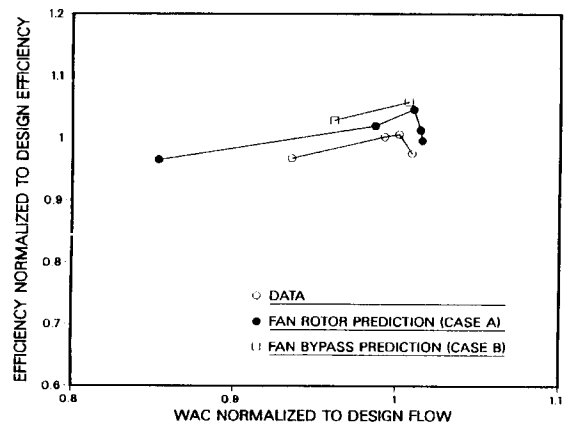

Figure 13. Comparison of measured and predicted mass-averaged adiabatic efficiency vs. flow (Case A & B).

6

data. In general, the predicted pressure ratios and efficiencies for Case B are slightly higher than that for Case A for all the fan operating points. The computed pressure ratio at a given airflow is greater than the data by 0.7% and 1.8% for Cases A and B respectively. Likewise, the predicted efficiency values are higher than the measured data by 3.6% for case A and 4.5% for Case B.

Figure 14 shows the predicted and measured spanwise variations of pitchwise mass-averaged normalized total pressure ratio at
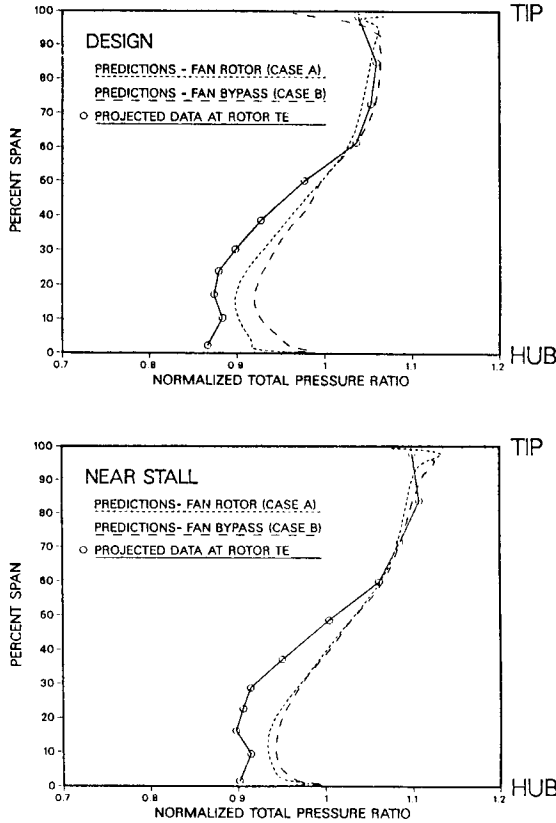

Figure 14. Predicted and measured spanwise variations of pitchwise mass-averaged pressure ratio (Case A & B).

the trailing edge of the rotor for Cases A and B. Figure 14 presents results for the fan design point and the near stall conditions. The variation in slope of total pressure ratio near hub and 20% span agrees well with the design intent. For Case B, the predicted pressure ratio deviated more than the projected data near the hub region. At the design point, the predicted total pressure ratio for Case B showed maximum difference of 2.6% than predicted values for Case A at the 10% streamline (from hub). Outboard of 55% span, the computed total pressure ratios compared well with data. For the near stall case, the predicted pressure ratio for Case A is closer to that of Case B. However, deduced data and the prediction differ from the hub to 50% span. As stated earlier, these descrepencies could possibly be due to numerics, turbulence model, or data transformation and need further investigation.

The spanwise variations of pitchwise-mass averaged relative flow angle at the rotor exit are shown for both fan cases in Figure 15. Also shown are angles deduced from test measurements at the design and near stall points. For the fan design point, relative to Case A, Case B predictions show the flow to be about 3 degrees closer to the axial direction at approximately 15% span. Between 50% to 70% span, the predicted flow angles for Case B show less turning (relative to Case A) by approximately 3 deg. Similar behavior is predicted for the near stall conditions. In general, the predicted flow angles are in fair agreement with the data.

The spanwise variations of normalized pitchwise mass-averaged efficiencies are compared with projected data at the rotor trailing edge in Figure 16 for Cases A and B at the fan design and near stall
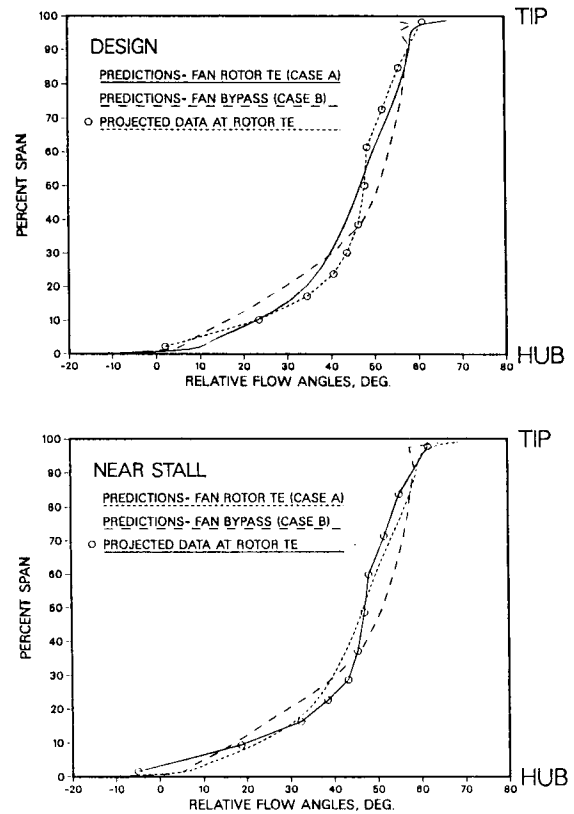

Figure 15. Predicted and measured spanwise variations of pitchwise mass-averaged relative flow angles (Case A & B).
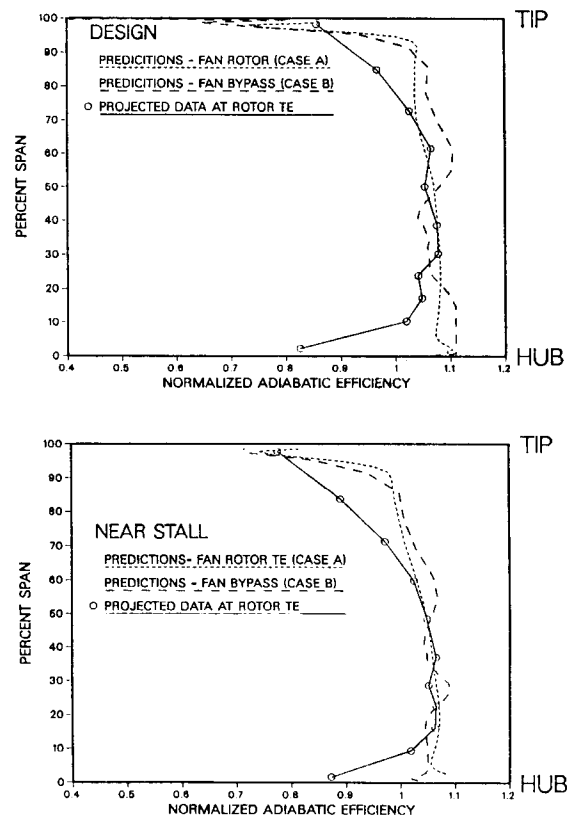

Figure 16. Predicted and measured spanwise variations of pitchwise mass-averaged adiabatic efficiency (Case A & B).

7

points. For both the flow conditions, the predicted efficiencies were above the data in the inboard 15% of the span and outboard of 70% span. At other spanwise locations, the predicted efficiencies compared reasonably well with the data.

The predicted normalized static pressure contours for Cases A and B are shown in Figure 17 at the mid-pitch meridional plane (at fan
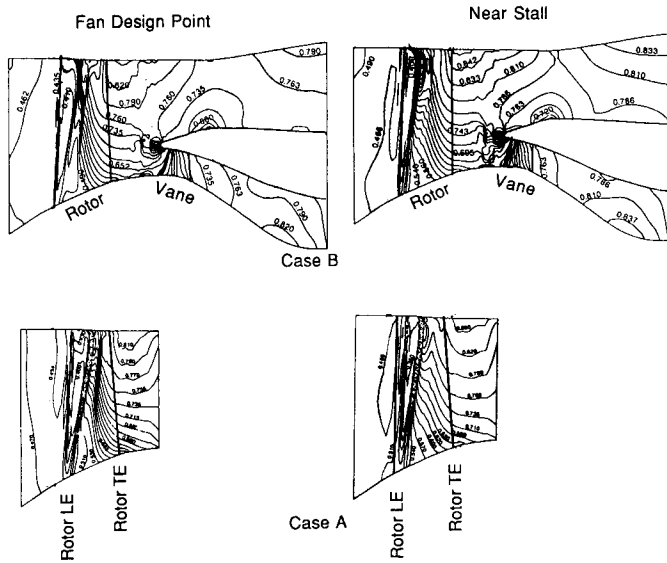

Figure 17. Predicted normaized static pressure contours in the meridional plane at mid-pitch (Case A & B).

operating point and near stall). The static pressures are normalized with respect to total pressure at the trailing edge of the fan rotor. The predicted pressures show some spatial oscillations (design point and near stall). These oscillations are caused by using minimium smoothing in the code to reduce the numerical loss. The solution is converged and oscillations are not due to flow unsteadiness. At mid pitch, the predicted pressures for Case A are slightly higher near the hub and lower in the tip regions as compared to Case B (for design point). The same is true for the near-stall conditions. It is observed that the large static pressure gradient shown in the plane of the splitter nose does not appreciably affect the static pressure distribution in the plane of the rotor blade trailing edge.

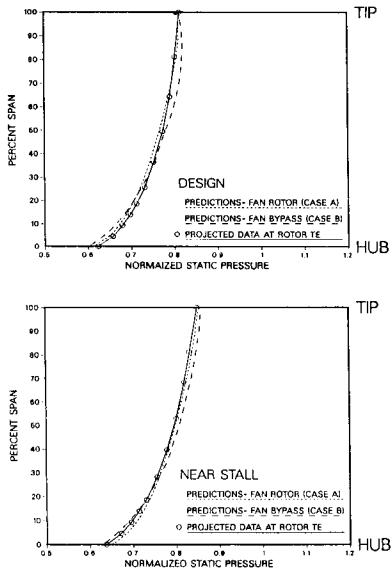Figure 18 compares spanwise variations of pitchwise mass-av-

Figure 18. Predicted and measured spanwise variations of pitchwise mass-averaged normalized static pressures at the rotor trailing edge (Case A & B).

eraged static pressure (normalized) at the rotor trailing edge for Case A, Case B, and as deduced from the test data. Distributions for the fan design point and at near stall are shown. The predicted static pressures are within ±1.8 percent of those obtained from the data.

Predicted normalized static pressure contours in the blade to blade plane of the fan bypass configuration is shown in Figure 19(a), (b),(c). The contours are shown for the fan design point and near stall
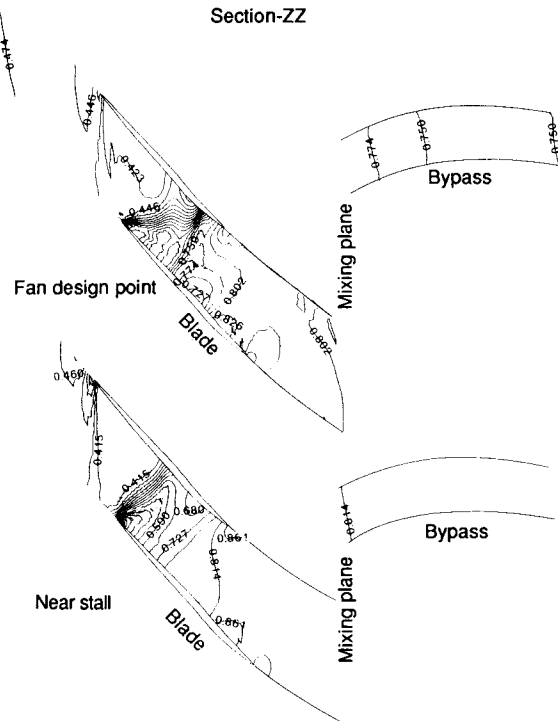

Figure 19(a). Normalized static pressure contours in blade to blade plane (Case B; design and near stall; at section-XX, YY, ZZ).
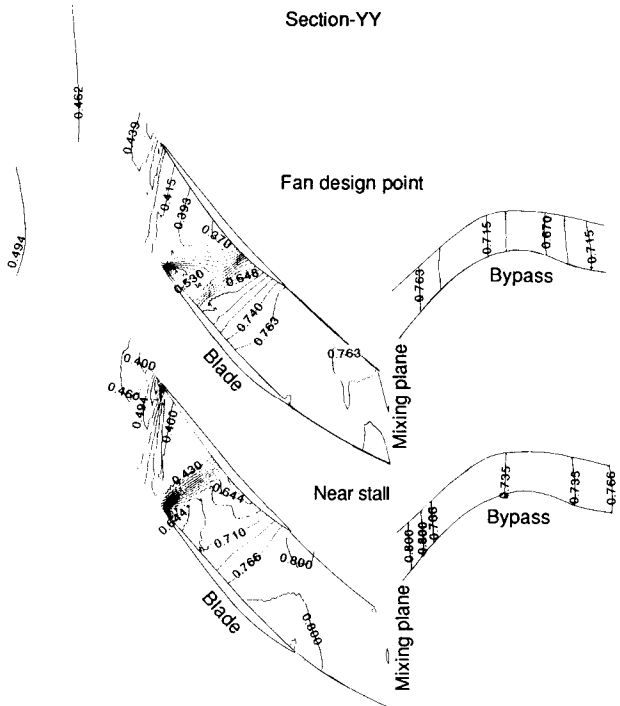

Figure 19(b). Normalized static pressure contours in blade to blade plane (Case B; design and near stall; at section-XX, YY, ZZ).
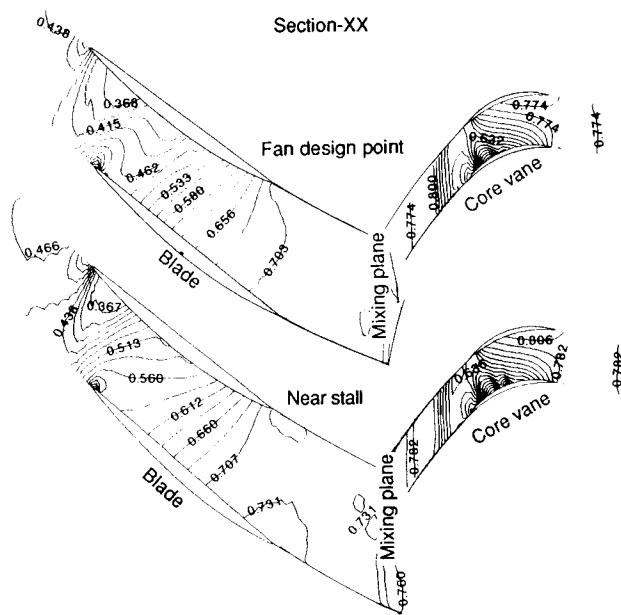
8

Figure 19(c). Normalized static pressure contours in blade to blade plane (Case B; design and near stall; at section-XX, YY, ZZ).

condition at three spanwise grid locations (XX, YY and ZZ shown in Figure 11). For the design point, the predicted static pressures at spanwise stations ZZ and YY show a bow shock followed by normal shock slightly upstream of the rotor trailing edge. There seems to be a slight difference in the shock pattern at 70% span between Case A (Figure 9) and Case B (section YY). In Case B a bow shock is followed by a normal shock, while in Case A the bow shock is not seen noticeably (note that Figure 9 is presented in terms of relative Mach numbers). For the near stall condition, the predicted static pressures at sections ZZ and YY show normal shock sitting near the leading edge of the rotor. For the fan design and near stall conditions (section-XX), a local supersonic bubble occurs at the suction surface downstream of the rotor leading edge and terminates to subsonic flow after a week shock (sonic Mach number at normalized pressure of 0.415).

Blade Tip Clearance Sensitivity

Table II shows results of the 3-D analysis at two levels of blade tip clearances, 0.04 inches and 0.08 inches. In the computations, only three nodes were used in the rotor tip clearance region of 0.04 in. and 0.08 in. Again, the study was very approximate and the purpose of the study was to predict the first-order effects in the tip clearance region of the fan rotor. These values of clearance were selected to be representative of the two levels of clearance which were experimentally investigated during rig tests of the fan. Predicted sensitivity to blade tip clearance generally tracks well with observed results for the clearances investigated.

Table-II.
Results of 3-D analysis at two levels of blade tip clearances.

	% change in flow parameters for rotor tip clearances of 0.04 inches and 0.08 inches (reference 0.04" clearance)	
	Data (%)	Predictions (%)
Rotor Pressure Ratio	1.21	0.962
Rotor Efficiency	1.68	1.940
Corrected Fan Flow	1.25	1.56

The flowfield through the core vane as predicted with the 3-D solver compared favorably with measured data, although these comparisons are not given here in an effort to confine the scope of this paper to the fan rotor.

CONCLUDING DISCUSSION

The generality and robustness of the Dawes 3-D Navier-Stokes solver has been demonstrated by application to an advanced fan bypass configuration. The detailed flow predictions were compared with the data in terms of design parameters at design and off-design conditions. An advanced engine fan design has been analyzed within reasonable computer resources. The analysis was used as a guide to modify the hardware which resulted in improving the fan efficiency by 2.5 percent.

In general, the predicted efficiency exceeded the measured value by about two and a half percentage points. The shapes of efficiency-flow and pressure ratio-flow characteristics were in good agreement with test data trends.

Even with the relatively simple tip clearance model used in the calculations, the predicted tip clearance effects agreed well with those observed in the data. The predicted pressures and efficiencies were higher than the data near in the near hub and tip regions. The source of these discrepencies is currently under investigation.

Due to the large axial gap between fan rotor and splitter, the splitter did not affect the performance of the rotor. However, the calculations are very important for the fan bypass configuration: first, the smaller axial gap may impact the performance of the fan rotor due to the presence of the splitter. Second, the core vanes are more effected by the performance of the upstream rotor.

REFERENCES

Dawes, W.N. (1991) "Multiblade row Navier-Stokes simulations of fan bypass configuration," ASME Paper 91-GT-148, 35th ASME Gas Turbine Conference, Orlando, Florida.

Adamczyk, J.J., Celestina, M.L., Beach, T.A. and Barnett,M (1989), "Simulation of three dimensional viscous flow within a multistage turbine," Trans. ASME J. of Turbomachinery presented at 89-GT-152 at the 34 International Gas Turbine Gas Turbine Conference, Toronto.

Cedar, R.D. and Holmes,D.G. (1989) "The calculation of the 3-D flow through fan including the effects of blade surface boundary layers, engine splitter and adjacent blade rows," ASME Paper 89-GT-325, 34th International Gas Turbine Conference, Toronto.

Dawes, W.N. (1988) "Development of a 3-D Navier-Stokes solver for application to all types of turbomachinery," ASME Paper 88-GT-70, 33rd International Gas Turbine Conference, Amstredam.

Baldwin, B. and Lomax, H. (1978) "Thin layer approximation and algebraic model for separated turbulent flows," AIAA Paper 78-257.

Dawes, W.N. (1987) "Analysis of 3-D viscous flows in transonic VKI compressors," VKI Lecture Series 3 Transonic Compressors, 1-4 Feb. 1987.

Adamczyk, J.J., Beach, M.L., Celestina, T.A. and Barnett, M. (1991), "Simulation of 3-D viscous flow within a multistage turbomachine," ASME Journal of Turbomachinery, Vol. 113, 1991.

Dring, R.P. and Spear, D.A. (1990) "The effects of wake mixing on compressor aerodynamics," ASME Paper 90-GT-132, 34th International Gas Turbine Conference, Brussels.

Stratford, B.S. (1959) "Prediction of separation of the turbulent boundary layer," JFM 5, 1-16.

Stores, J.A. and Cumpsty, N.A. (1991) "Tip leakage flow in axial compressor," ASME Journal of Turbomachinery, Vol. 113, April 1991.

Basson, A.H., Kunz, R.F. and Lakshminarayan, B. (1991) "Grid generation for three dimensional turbomachinery geometries including tip clearance," AIAA Paper 91-2360, AIAA/SAE/ASME 27th Joint Propulsion Conference, Sacramento 1991.

9